14th International Symposium on Turbulence and Shear Flow Phenomena (TSFP14)
Heidelberg, Germany, July 28–31, 2026

SMOOTH-TO-ROUGH-TO-SMOOTH: EFFECTS OF FINITE ROUGHNESS FETCH UPSTREAM OF A ROUGH-TO-SMOOTH STEP CHANGE.

Martina Formichetti
Aeronautical and Astronautical Engineering
University of Southampton
Burgess Rd, SO16 7QF, Southampton, UK
martina.formichetti@soton.ac.uk

Dea D. Wangsawijaya
Aeronautical and Astronautical Engineering
University of Southampton
Burgess Rd, SO16 7QF, Southampton, UK
d.d.wangsawijaya@soton.ac.uk

Sean Symon
Aeronautical and Astronautical Engineering
University of Southampton
Burgess Rd, SO16 7QF, Southampton, UK
sean.symon@soton.ac.uk

Bharathram Ganapathisubramani
Aeronautical and Astronautical Engineering
University of Southampton
Burgess Rd, SO16 7QF, Southampton, UK
g.bharath@soton.ac.uk

ABSTRACT

Step changes in surface roughness have been widely studied, but the role of finite fetch and sequential step-changes remains unclear. Building on Formichetti *et al.* (2025), which quantified equilibrium recovery of a turbulent boundary layer (TBL) after a smooth-to-rough step, we extend the setup to a smooth-to-rough-to-smooth sequence. We examine how non-equilibrium incoming TBLs, set by a finite roughness fetch L, affect the initial condition at the rough-to-smooth step and the early recovery. In a zero-pressure-gradient TBL over P24 sandpaper, L/δ_2 is varied from 1 to 39 (δ_2 being the mean TBL thickness of the longest-fetch case at the drag balance location) across $4\times10^3 \le Re_\tau \le 2\times10^4$. Velocity fields are acquired from the rough-to-smooth step to approximately $2\delta_2$ downstream. We show that while longer fetches observe a classic single inner layer, short fetches produce two internal layers after the rough-to-smooth change: a smooth-wall layer and a displaced log region set by the earlier roughness, which diminishes with distance. Reynolds shear stress profiles exhibit a similar trend with visibly sharper inflection points than mean velocity profiles.

1 INTRODUCTION

TBLs over rough surfaces occur in many engineering and environmental flows. For homogeneous rough walls, drag and structure are well described through the friction velocity u_τ and equivalent sand-grain roughness k_s (Jiménez, 2004). In practice, k_s is inferred from the fully rough log law (Nikuradse, 1950; Colebrook *et al.*, 1937).

However, real surfaces are rarely uniform. Abrupt step changes, such as patches of biofouling or land-use transitions, disrupt equilibrium and generate internal layers (ILs) that grow downstream. After a step change in roughness, the IL development alters the structure of the TBL by replacing the single log region with a blend of two: a lower layer in local equilibrium with the new surface and an outer layer that retains equilibrium with the upstream surface (Elliott, 1958; Townsend, 1965). These steps also trigger overshoots or undershoots in wall shear stress (WSS) (Bradley, 1968; Antonia & Luxton, 1971, 1972; Efros & Krogstad, 2011; Hanson & Ganapathisubramani, 2016), with recovery lengths reported to vary widely depending on the diagnostic used. A roughness patch has two roughness transitions: a smooth-to-rough (S $\rightarrow$ R) upstream edge followed by a rough-to-smooth (R $\rightarrow$ S) transition downstream and each transition has its own internal layer. Previous work has only focussed on short patches with arbitrary lengths (typically $L \le 3\delta$, where L is the length of the patch and δ is the local boundary layer thickness at the interface) and demonstrated the presence of a "stress-bore" due to interacting ILs that have long recovery distances over 55δ (Andreopoulos & Wood 1982; Smits & Wood 2001; Jacobi & McKeon 2011). In this work, we build on Formichetti *et al.* (2025) where we determined equilibrium fetch requirements after a R $\rightarrow$ S step-change, we now examine the subsequent R $\rightarrow$ S transition. Our goals are to assess how finite upstream fetch L sets the initial condition at the R $\rightarrow$ S step, to investigate the sensitivity of different turbulent structures to this transition in the near field, and to determine how the structural response develops downstream. In the future, we also aim to test whether a k_s-based description remains valid in this non-equilibrium context. We hypothesise that k_s decays gradually towards zero downstream of the second step, with the decay rate depending on L.

This submission will cover the methodology used in §2, the preliminary results in §3, and early conclusions and future plans in §4.

2 METHODOLOGY

This study extends the experimental campaign of Formichetti *et al.* (2025), carried out in the University of Southampton's boundary layer wind tunnel (BLWT). That study measured WSS with a floating-element drag balance and PIV to quantify equilibrium recovery after a smooth-to-rough step. The balance, described by Ferreira *et al.* (2024), was located $59\delta_2$ downstream of the inlet and directly measured skin friction during velocity sweeps ($10 \le U_\infty \le 40\,\mathrm{ms}^{-1}$) with $< 1\%$ uncertainty.

The present study targets the region downstream of the roughness, where the surface returns to smooth. This creates a second step change and allows assessment of how L influences both the near-step condition and recovery over $2\delta_2$. The roughness consists of P24 sandpaper patches ($2\delta_2 \times 8\delta_2$), taped sequentially upstream so that L/δ_2 varies from 1 to 39 (figure 1).

Flow development is characterised using planar PIV at $U_\infty = 20$ ms^{-1}. The field of view, centred on the balance, spans $\approx 6\delta_2 \times 1.5\delta_2$ in the streamwise x and wall-normal y directions (Figure 1). Images were acquired with two LaVision Imager CMOS 25 MP cameras (17 px/mm) and a dual-cavity Nd:YAG laser (200 mJ, 532 nm). Data were sampled at 1 Hz for 2000 snapshots and processed with an in-house algorithm using 16×16 px windows with 75% overlap, yielding $\Delta x^+ \times \Delta y^+ \approx 30 \times 30$. The mean velocity uncertainty is $\sim 2\%$.

To extract integral length scales from spatial correlation maps, a parametric fitting methodology was employed. Two-point correlations of the streamwise velocity fluctuations, R_{uu}, were computed at four varying wall-normal reference heights, as depicted in Figure 2. Following a Gaussian smoothing to mitigate local PIV noise, correlation contours were extracted at specific thresholds ($\rho = 0.2$ for large-scale motions (LSM), and $\rho = 0.5$ for small-scale motions (SSM)). A parametric ellipse was subsequently fitted to the primary contour using non-linear least squares, providing a globally smooth estimate of the structure's geometry. Finally, to ensure physical validity, this fit was mathematically constrained by masking any regions extending below the wall ($y = 0$), guaranteeing that the extracted length scales accurately reflect physical dimensions.

3 RESULTS

Figure 3 shows the mean streamwise velocity field for the shortest fetch case, with flow from left to right. The incoming smooth-wall TBL encounters a smooth-to-rough step where the sandpaper begins, develops over a rough length of $\approx 2\delta_2$, and finally passes a rough-to-smooth step followed by $\approx 2\delta_2$ of smooth-wall recovery. This configuration highlights the sequential step-change arrangement used in this study. Also marked are the three PIV sampling stations (S1, S2, S3), located downstream of the second step and spaced $\approx 0.8\delta_2$ apart. These stations provide data on the early recovery process, allowing us to analyse the early evolution of the TBLs after the second step-change.

$1\delta_2$	$3\delta_2$	$5\delta_2$	$7\delta_2$	$9\delta_2$	$19\delta_2$	$39\delta_2$
▼	▼	▼	▼	▼	▼	▽

Table 1. Colour legend for different roughness fetches upstream of the rough-to-smooth step-change scaled by δ_2 - the TBL thickness at the drag balance location for the longest fetch case.

Figure 4 presents the mean velocity profiles at S1, S2, and S3 for varying upstream fetches (colour scheme in table 1). The data are normalised with the drag-balance friction velocity upstream of the second step ($u_{\tau,DB}$) and the equivalent sand-grain roughness height ($k_{s,DB}$) obtained using the internal layer fitting method of Formichetti *et al.* (2025) also for the TBLs above the drag balance. At S1, directly at the step, finite fetch length strongly influences the profiles. Mid-fetch cases ($3\delta_2$–$19\delta_2$) display two distinct inflection points: one associated with the new smooth-wall IL initiated at the second step, and another reflecting the displaced IL generated by the upstream smooth-to-rough transition. This behaviour confirms that the downstream flow retains memory of the finite fetch upstream. As fetch increases, the "older" IL is progressively displaced outward and weakened, while the new IL grows from the wall. The collapse of mid-fetch profiles at higher wall-normal locations suggests that, above a certain height, the flow becomes less sensitive to upstream fetch, consistent with classical IL theory. With distance downstream (S2, S3), the inflection points shift upwards, indicating IL growth and the gradual reorganisation of the boundary layer. This trend is most clearly seen in the $3\delta_2$ fetch case, where the blending of the two ILs produces the most noticeable distortion.

Figure 5 shows the corresponding Reynolds shear stress ($-\overline{u'v'}$) profiles, scaled with $u_{\tau,DB}$ and the local boundary-layer thickness δ_{99} at the sampling locations S1, S2, and S3. The influence of upstream fetch is again evident. At S1, the presence of two ILs is clearly marked by two inflection points in the Reynolds shear stress distribution over wall-normal distance. This is consistent with the concept of a "stress-bore" indentified by Smits & Wood (2001). With increasing fetch, the imprint of the upstream IL weakens as equilibrium is re-established upstream of the second step-change, and in the longest case, it completely disappears. Moving downstream to S2 and S3, the effect of finite fetch weakens as the new IL grows and the turbulence transitions toward a single-IL organisation. The most noticeable change is once again displayed by the $3\delta_2$ case at increasing distance from the second step-change. Here, we can clearly see the IL from the R $\rightarrow$ S step change grow within the TBL outwards with distance from the transition. These results demonstrate that the recovery after a R $\rightarrow$ S step is not universal but depends strongly on the upstream fetch length.

To characterise the flow stuctures associated with non-equilibrium recovery of the TBL, two-point correlations of the streamwise velocity fluctuations, R_{uu}, were computed. Ellipses are fitted to the contours of two-point correlations and these are examined at the three downstream stations (S1, S2, and S3). These contours are evaluated at two representative wall distances, $y_{\text{ref}} = 0.04\delta_2$ and $0.16\delta_2$, which correspond to the regions where the logarithmic profile breaks into a newly forming inner layer and a displaced outer layer. Two different contours levels are chosen for examination with a contour level of 0.3 to represent Large Scale Motions (LSMs) and a level of 0.5 to represent Smaller Scale Motions (SSMs) of the flow. Ideally, a lower contour level should be chosen for the LSMs but there is balance between the number of fields required for converged statistics and the signal level. As a compromise, a low enough value but that represents the larger scales is chosen. Comparing the LSMs in Figure 6 against the SSMs in Figure 7 reveals a stark contrast in structural adaptation. The SSM contours (Figures 7a and 7b) remain highly compact and relatively invariant, demonstrating almost no sensitivity to either the downstream progression or the upstream history. In contrast, LSMs (Figures 6a and 6b) exhibit a great spatial distortion that is highly dependent on the wall-normal distance. In the inner log region ($y_{\text{ref}} = 0.04\delta_2$, Figure 6a), the LSM ellipses are clearly elongated in the streamwise direction, representing the chaotic stretching of the re-establishing near-wall structures. Meanwhile, in the outer log region ($y_{\text{ref}} = 0.16\delta_2$, Figure 6b), the contours become noticeably more inclined and vertically expanded. Moreover, the extent of these spatial distortions seems dependent on the upstream fetch. For short roughness fetches, the stretching is more pronounced and persistent from S1 through S3. Conversely, for longer fetches, where the incoming turbulent structures have achieved equilibrium prior to the transition, the correlation shapes are significantly less distorted and undergo a much smoother, damped structural adjustment across the measurement stations.

In order to better inspect the effects of the step-change and the upstream roughness fetch on the turbulent structures, the integral length scale L_x was extracted from the correlation maps to quantify the streamwise extent and wall-normal height of the turbulent structures. Following an impulsive perturbation, integral length scales are significantly suppressed in the near-wall region whilst simultaneously undergoing inflation further from the wall as observed in Jacobi & McKeon (2011). This behaviour is directly evident in the present data: immediately downstream of the step change, the near-wall integral scales ($y_{\mathrm{ref}} = 0.02\delta_2$ and $0.04\delta_2$ in Figure 8a and Figure 8b) drop notably below the smooth-wall baseline. Conversely, in the outer region ($y_{\mathrm{ref}} = 0.16\delta_2$), there is a substantial inflation of these scales, as seen in Figure 8a. This inflation characterises the physical displacement of larger structures away from the wall and into the outer flow, where they persist whilst smaller scales remain confined closer to the wall during the protracted recovery phase.

The isolation of integral scales into LSMs and SSMs reveals a significant scale decoupling during the relaxation process. Whilst the outer-layer LSMs in Figure 8a are heavily perturbed, inflating to over twice their equilibrium size before gradually decaying, the SSMs at the equivalent wall-normal height in Figure 8b remain largely unaltered, sustaining a ratio close to unity. This indicates that small-scale structures adjust almost instantaneously to the new local boundary condition. In contrast, the large-scale structures retain a strong historical memory of the upstream roughness, thereby dictating the prolonged, non-equilibrium recovery of the boundary layer. This disparity likely arises because the small-scale structures, being situated closer to the wall and possessing shorter turnover times, are continually regenerated by the local, smooth-wall boundary condition. In contrast, the large-scale motions, populated by energetic structures displaced from the upstream roughness, reside in the outer region where dissipative time scales are significantly longer, thereby preserving the structural mark of the finite fetch.

The introduction of varying upstream fetch lengths bridges the critical gap between an isolated spatial impulse and a transition between fully developed equilibrium states. Short roughness fetches ($\approx 1\delta_2$) act as a structural shock to the incoming flow, resulting not only in the most pronounced outer-layer scale inflation but also in a distinct overshoot during the near-wall recovery ($y_{\mathrm{ref}} = 0.02\delta_2$ in Figure 8a). Conversely, a prolonged roughness fetch ($\approx 39\delta_2$) permits the turbulent structures to achieve a more settled state prior to the rough-to-smooth step change. This incoming condition yields a heavily damped, stable relaxation trajectory, thus avoiding the severe shock and subsequent overshoot observed in the short-fetch cases. Consequently, these results demonstrate that the severity of the downstream structural displacement is fundamentally governed by the development and equilibrium condition of the upstream rough TBL.

4 CONCLUSIONS

This study demonstrates that the recovery of a TBL following a rough-to-smooth step change depends fundamentally on the upstream roughness fetch. Short fetches act as a structural shock, producing a complex double-layer structure characterised by an overshoot in the near-wall scales and a severe inflation of displaced structures persisting above. This recovery exhibits a distinct scale decoupling: whilst SSMs adapt almost instantaneously to the new local boundary condition, LSMs retain a strong historical memory of the upstream roughness. With increasing fetch, the incoming flow reaches equilibrium before facing the rough-to-smooth step-change, which significantly diminishes these non-equilibrium effects and yields a heavily damped, stable relaxation trajectory. These results indicate that sequential step changes cannot be simply modelled as an immediate reset to smooth-wall conditions. Future work will quantify the growth and decay of these interacting layers, compare the findings with canonical rough-to-smooth configurations, and test the suitability of a local k_s framework for simulating such complex flows.

Acknowledgements

The authors acknowledge funding from the Leverhulme Early Career Fellowship (Grant ref: ECF-2022-295), the European Office for Airforce Research and Development (Grant ref: FA8655-23-1-7005) and EPSRC (Grant ref no: EP/W026090/1).

REFERENCES

Andreopoulos, J. & Wood, D. H. 1982 The response of a turbulent boundary layer to a short length of surface roughness. *J. Fluid Mech.* **118**, 143–164.

Antonia, R. A. & Luxton, R. E. 1971 The response of a turbulent boundary layer to a step change in surface roughness Part 1. Smooth to rough. *J. Fluid Mech.* **48** (4), 721–761.

Antonia, R. A. & Luxton, R. E. 1972 The response of a turbulent boundary layer to a step change in surface roughness Part 2. Rough to smooth. *J. Fluid Mech.* **53** (4), 737–757.

Bradley, E. F. 1968 A micrometeorological study of velocity profiles and surface drag in the region modified by a change in surface roughness. *Q. J. R. Meteorol. Soc.* **94**, 361—-379.

Colebrook, C. F., White, C. M. & Taylor, G. I. 1937 Experiments with fluid friction in roughened pipes. *Proc. R. Soc. Lond. Series A* **161** (906), 367–381.

Efros, V. & Krogstad, P. 2011 Development of a turbulent boundary layer after a step from smooth to rough surfaces. *Exp. Fluids* **51**, 1563–1575.

Elliott, W. P. 1958 The growth of the atmospheric internal boundary layer. *Eos Trans.* **39** (6), 1048–1054.

Ferreira, M. A., Costa, P. & Ganapathisubramani, B. 2024 Wall shear stress measurement using a zero-displacement floating-element balance. *Exp. Fluids* **65** (56).

Formichetti, M., Wansawijaya, D. D., Symon, S. & Ganapathisubramani, B. 2025 Effects of fetch length on turbulent boundary layer recovery past a step change in surface roughness. *J. Fluid. Mech.* **1009**, A66.

Hanson, R. E. & Ganapathisubramani, B. 2016 Development of turbulent boundary layers past a step change in wall roughness. *J. Fluid Mech.* **795**, 494–523.

Jacobi, I. & McKeon, B. J. 2011 New perspectives on the impulsive roughness-perturbation of a turbulent boundary layer. *J. Fluid Mech.* **677**, 179–203.

Jiménez, J. 2004 Turbulent flows over rough walls. *Ann. Rev. Fluid Mech.* **36**, 173–196.

Nikuradse, J. 1950 Laws of flows in rough pipes .

Smits, A. J. & Wood, D. H. 2001 The flow over rough surfaces. *Ann. Rev. Fluid Mech.* **33**, 321–347.

Townsend, A. A. 1965 The response of a turbulent boundary layer to abrupt changes in surface conditions. *J. Fluid Mech.* **22** (4), 799–822.

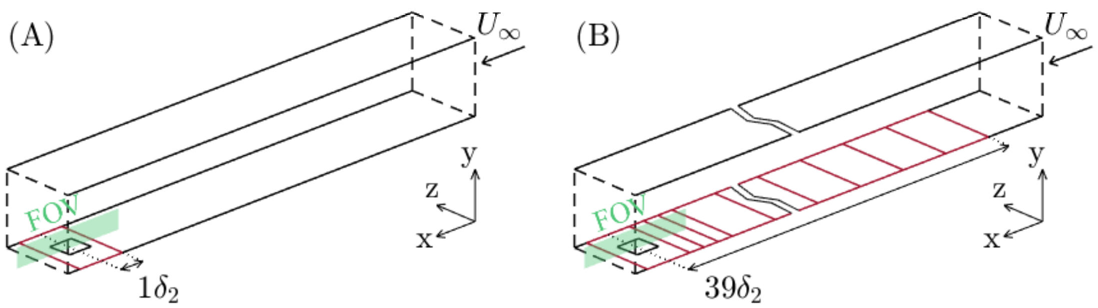

Figure 1. Experimental set-up schematic with varying roughness fetch length L measured from the drag balance centreline. Shortest fetch case in (A) and longest fetch case in (B).

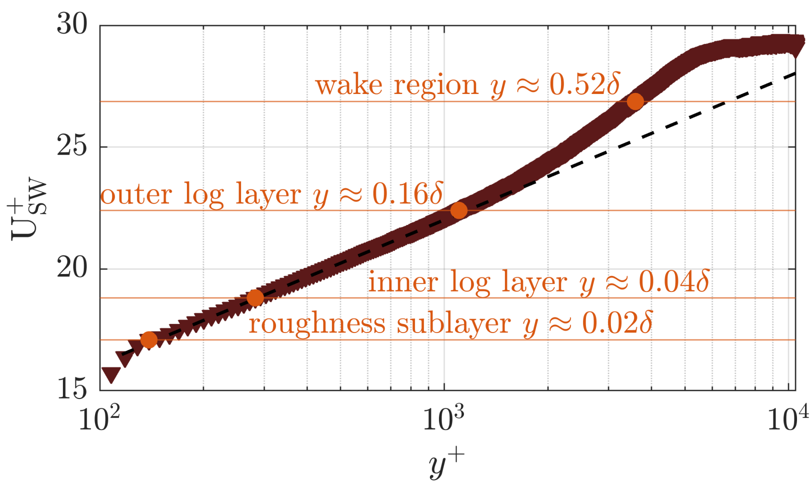

Figure 2. Depiction of the 4 wall distances used as reference to compute 2D correlations on a smooth-wall TBL mean-velocity profile plotted against wall distance in viscous units. The profile was sampled upstream of the roughness, and the u_τ used for normalisation was found by fitting the log profile.

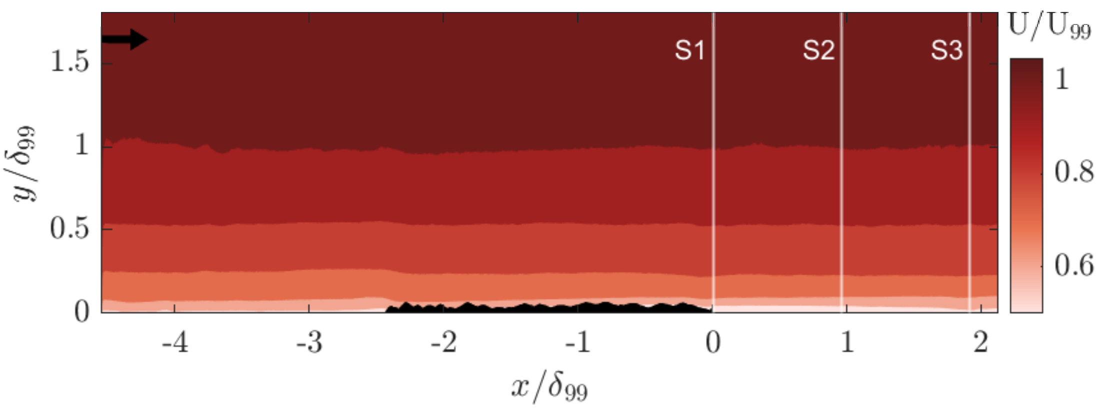

Figure 3. Mean streamwise velocity contour for the shortest roughness fetch case displaying the sampling locations after the rough-to-smooth step-change - S1, S2, S3.

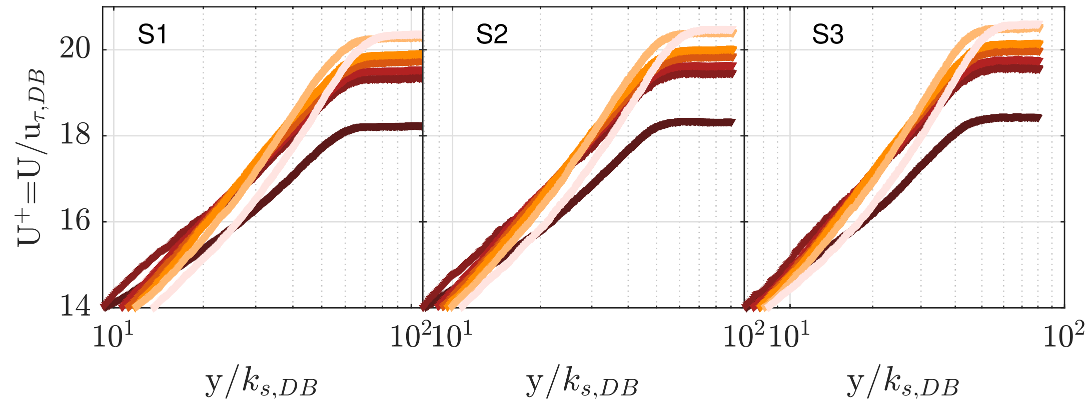

Figure 4. Mean streamwise velocity profiles at three sampling locations after the R → S step-change - S1, S2, S3. Velocity is normalised by $u_{\tau,DB}$ measured by the drag balance. Wall-normal distance is normalised by $k_{s,DB}$ computed at the drag balance location.

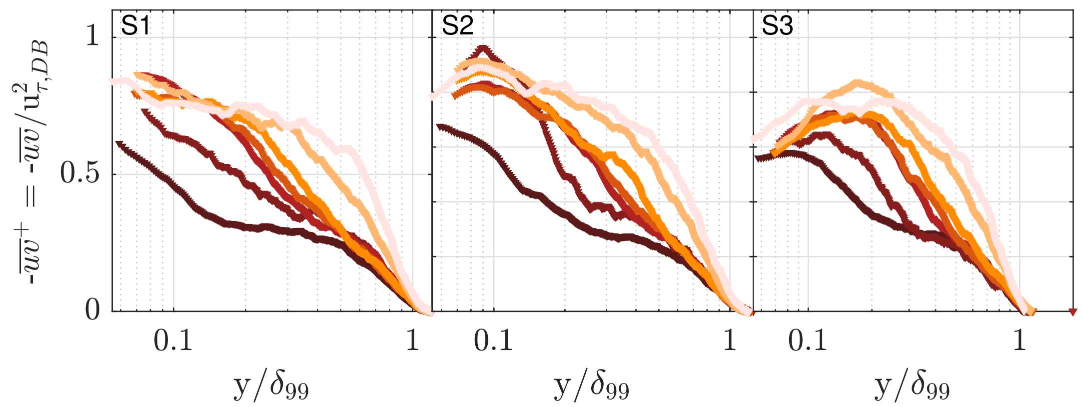

Figure 5. Reynolds shear-stress in viscous units (scaled by $u_{\tau,DB}$ measured by the drag balance) at three sampling locations after the R → S step-change - S1, S2, S3. Wall normal distance is normalised by local δ_{99}.

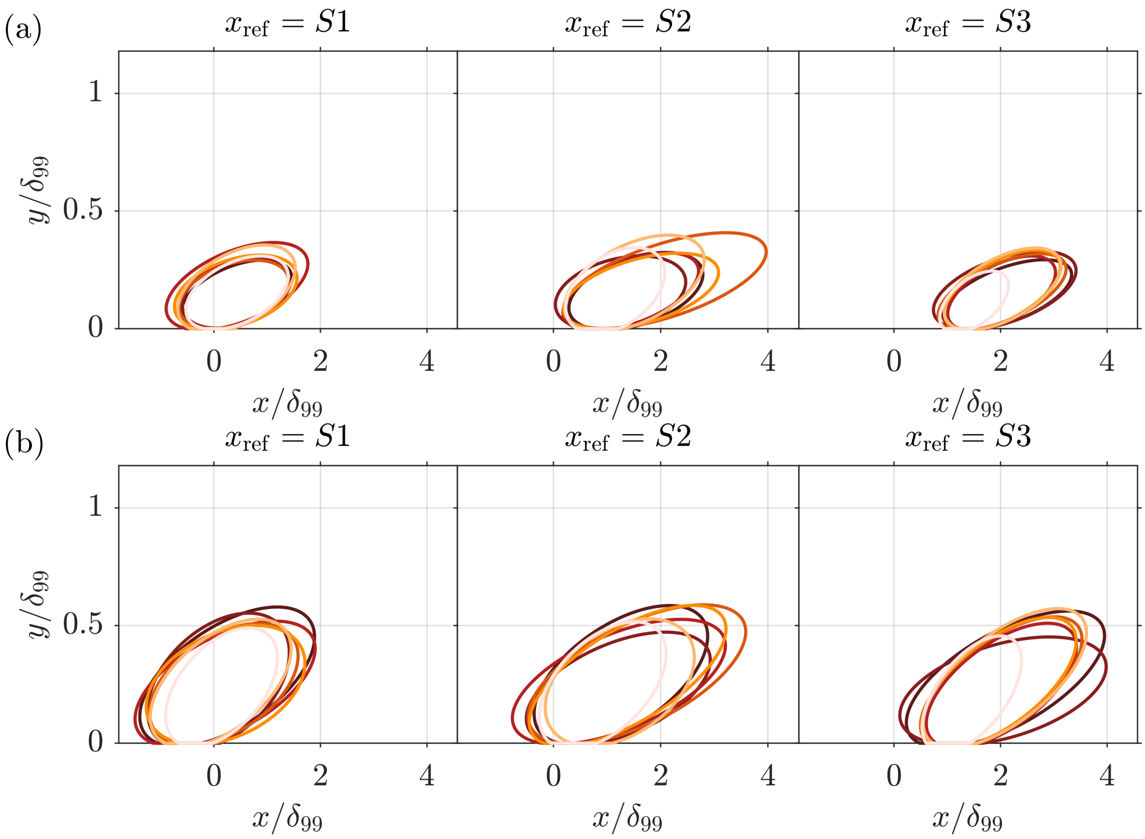

Figure 6. Elliptical fits of the 2D spatial correlation contours for a threshold $\rho = 0.2$, computed at three downstream locations S1, S2, S3, and two representative wall distances (a) $0.04\delta_2$ and (b) $0.16\delta_2$.

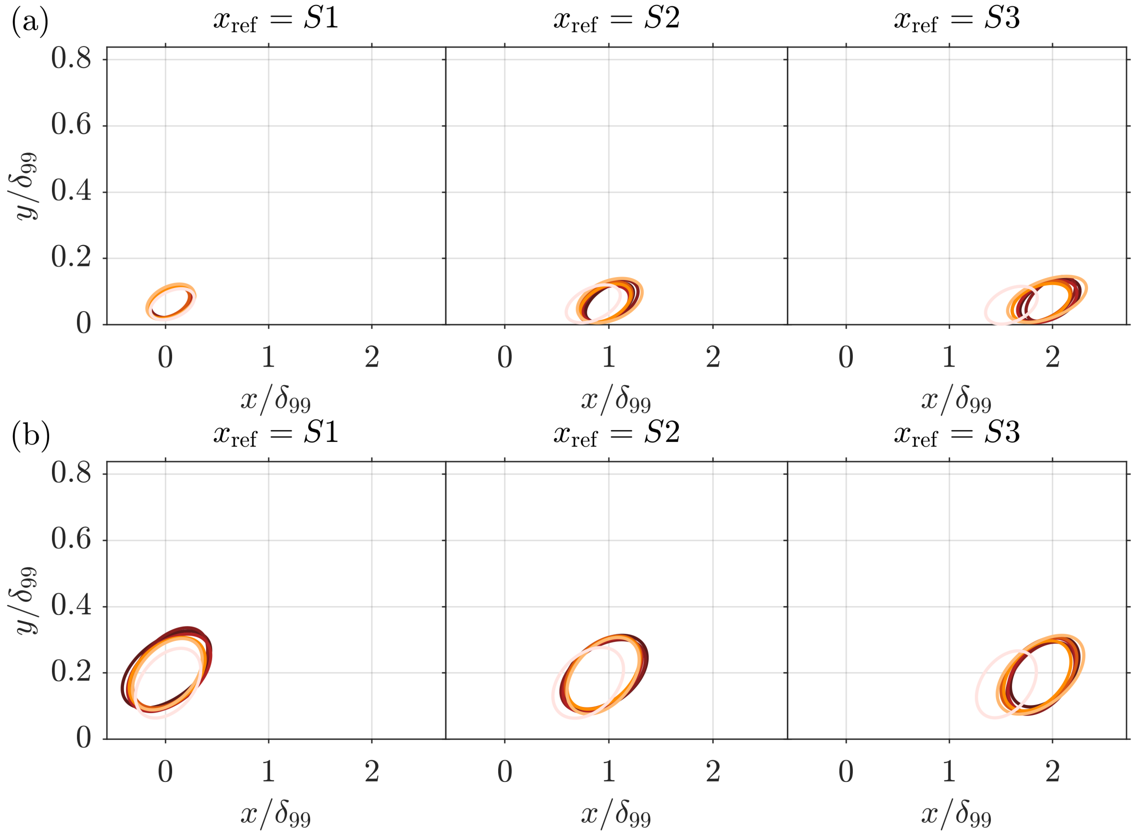

Figure 7. Elliptical fits of the 2D spatial correlation contours R_{uu} for a threshold $\rho = 0.5$, computed at three downstream locations S1, S2, S3, and two representative wall distances (a) $0.04\delta_2$ and (b) $0.16\delta_2$.

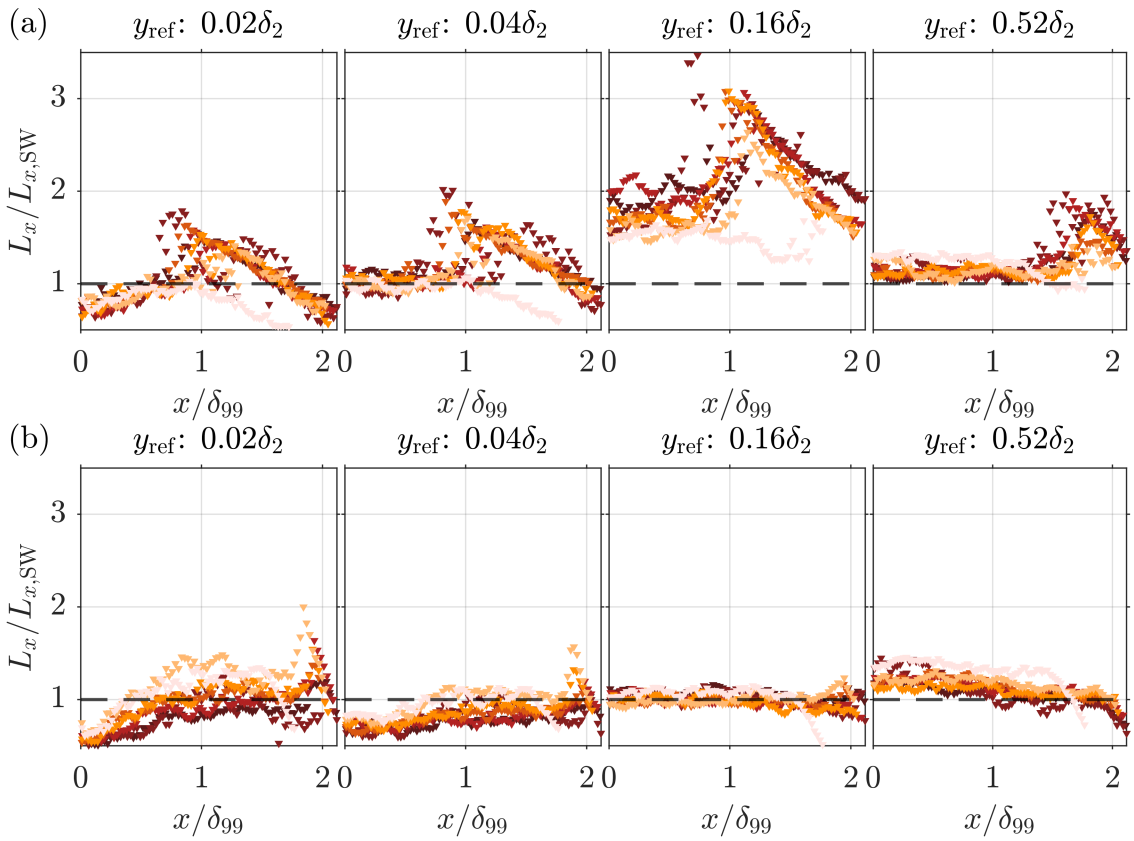

Figure 8. Integral length L_x (normalised by the L_x over a smooth wall at equivalent Re_τ) computed from 2D correlation R_{uu} at thresholds (a) 0.2 and (b) 0.5 plotted against streamwise distance, x, normalised by local δ_{99}.